Journal Pre-proof

Gas phase electronic spectra of xylene-water aggregates

Jack E. Fulker, Alejandro Gutiérrez-Quintanilla, Wendy A. Brown, Gustavo A. Pino, Antoine Hacquard, Ana Niedojadlo, Jennifer A. Noble

PII: S0022-2852(23)00026-7
DOI: https://doi.org/10.1016/j.jms.2023.111761
Reference: YJMSP 111761

To appear in: *Journal of Molecular Spectroscopy*

Received date : 20 December 2022
Revised date : 22 February 2023
Accepted date : 28 February 2023

Please cite this article as: J.E. Fulker, A. Gutiérrez-Quintanilla, W.A. Brown et al., Gas phase electronic spectra of xylene-water aggregates, *Journal of Molecular Spectroscopy* (2023), doi: https://doi.org/10.1016/j.jms.2023.111761.

Gas phase electronic spectra of xylene-water aggregates

Jack E. Fulker[1], Alejandro Gutiérrez-Quintanilla[‡2], Wendy A. Brown[*1], Gustavo A. Pino[3,4,5], Antoine Hacquard[§2], Ana Niedojadlo[3,4,5], and Jennifer A. Noble[*2]

[1]Department of Chemistry, University of Sussex, Falmer, Brighton, BN1 9QJ, UK; E-mail: w.a.brown@sussex.ac.uk
[2]Physique des Interactions Ioniques et Moléculaires (PIIM): CNRS, Aix-Marseille Université, Marseille, France; Email: jennifer.noble@univ-amu.fr
[3]INFIQC: Instituto de Investigaciones en Fisicoquimica de Córdoba (CONICET - UNC) - Haya de la Torre s/n Ciudad Univeritaria X5000HUA Córdoba, Argentina
[4]Departamento de Fisicoquimica, Facultad de Ciencias Quimicas Universidad Nacional de Córdoba - Haya de la Torre y Medina Allende Ciudad Univeritaria X5000HUA Córdoba, Argentina
[5]Centro Láser de Ciencias Moleculares - Universidad Nacional de Córdoba - Haya de la Torre s/n Pabellón Argentina, Ciudad Univeritaria X5000HUA Córdoba, Argentina

Abstract

Using a jet spectroscopy molecular beam setup, gas phase electronic spectra of three xylene isomers (*para*, *meta* and *ortho*) have been collected for the neutral monomer species as well as for their clusters with one and two water molecules. Scans at a resolution of ±0.02 nm showed a clear 0-0 transition for each xylene isomer as well as the vibronic progression. The spectra were assigned with the help of Franck-Condon factor PGOPHER simulations from theoretical studies at the CAM-B3LYP/aug-cc-pVDZ level of theory. The vibronic spectra of the xylene·H_2O and xylene·$(H_2O)_2$ clusters showed broad features between 36800-38400 cm^{-1} (260-272 nm) for *p*- and *m*-xylene, while the water clusters of *o*-xylene gave more defined bands. The separation of the vibronic bands in the clusters mirrors the progression of the neutral monomers implying that, for the $S_1 \leftarrow S_0$ transition, it is the same vibrational modes that are involved in the monomer as in the clusters with water. Both the separation and the spectral width of the bands can be explained by the calculated differences in geometries of the clusters in the ground and first electronic excited states.

1 Introduction

Xylene molecules ($(CH_3)_2C_6H_4$) are pollutants that are released in emissions from combustion processes and industrial solvents and they are also important precursors in the soot formation process during fuel combustion.[1–4] Due to their role as atmospheric pollutants, understanding their interaction with water molecules is very important. The role of water- and xylene-containing aggregates is also important in micelle formation.[5] Away from Earth, small aromatic molecules such as xylene are thought to play an important role in acting as building blocks for the formation of carbonaceous dust grains in space.[6–8] Such grains are often covered in layers of water ice, and hence the interaction of xylene with water is also important in non-terrestrial environments.[9]

Xylene is part of a family of aromatic molecules that also contains benzene and toluene. The addition, and relative position, of methyl groups on the benzene (toluene = CH_3, xylene = $(CH_3)_2$) affects both the shape and size of the molecule.[10] The polarity of each xylene isomer varies, with the *para* species being apolar (it has no dipole moment), *m*-xylene having a dipole moment of 0.35 D and *o*-xylene having a dipole moment of 0.64 D.[10,11] This change in dipole moment influences how water molecules approach the aromatic ring system of the xylenes, and therefore dictates how the species bind to each other during cluster formation. These changes then have an effect on the electronic properties of the species and therefore dictate how the molecules interact with other systems. This is of particular interest when considering how the xylene species bind to water to form aggregates, a common-phenomenon in atmospheric chemistry and astrochemistry.[1,12]

Xylenes are well-studied molecules in the gas phase, with the vibrational progression in the S_1 electronic excited state around 270 nm having been characterised by different groups using multiple spectroscopic techniques: resonant two-photon ionisation (R2PI) by Blease et al.,[13,14] dispersed emission (DE) by Breen et al.[15] and laser induced fluorecence (LIF) by Ebata et al.[16] More recently, the S_2 electronic excited states of xylene monomers have been studied due to

‡Present address: Université de Pau et des Pays de l'Adour, E2S UPPA, CNRS, IPREM, Pau, France
§Present address: Sorbonne Université, Observatoire de Paris, PSL University, CNRS, LERMA, F-75014, Paris, France

their ultra-fast lifetimes.[17,18] However, to the best of our knowledge, electronic spectra of xylene-water clusters have not yet been published in the literature. Infrared ion depletion spectroscopy of *p*-xylene·$(H_2O)_n$ clusters in the 3 μm region has revealed that the *p*-xylene·$(H_2O)_2$ cluster has a ground state geometry with a water dimer attached to the side of the aromatic ring, with the binding of the water trimer and tetramer being very similar.[19] On the other hand, the R2PI spectrum of *p*-xylene·NH_3 shows similar band progressions to the *p*-xylene monomer, demonstrating how influential the clustering species can be on the vibrational levels of these xylene clusters.[20]

Previous studies of neutral aromatic species have permitted the development of a simple physical model describing excited state dynamics of substituted aromatics ($\pi\pi^*/\pi\sigma^*$ coupling) which was subsequently also found to be successful in describing protonated systems.[21–23] The excited state model has also been successfully applied to a study of the reactivity of "soft" UV-induced polycyclic aromatic hydrocarbons (PAHs) with water clusters, where it was shown for the first time that the presence of water molecules in interaction with a neutral PAH molecule lowers the $\pi\pi^*/\pi\sigma^*$ energy gap. This allows the system to access the H-loss dissociation channel, and thus react to form an oxygenated PAH without ionising the PAH.[24,25] In this way, solvation of an aromatic system can fundamentally change its molecular physics.[10,11]

In light of this, the neutral monomer and water clusters of each of the xylene isomers have been studied in this work using photoionisation spectroscopy to investigate how the clusters behave in the gas phase. Furthermore, computational studies of the clusters have been performed to justify and explain the experimental observations. These calculations reveal how the geometries of both the monomers and clusters change during the $S_1 \leftarrow S_0$ transition, and the nature of the intermolecular interactions present in the complexes.

2 Methods

The molecular beam experiment is composed of two independently pumped vacuum chambers (base pressure = 10^{-6} mbar) separated by a 6 mm diameter skimmer. Helium carrier gas (2 - 6 bar) picks up the test species (xylene and water) from a reservoir and the mixture of products is expanded through the 200 μm nozzle of a pulsed valve (10 Hz, General Valve) into the first chamber.

In the second chamber, a homemade time-of-flight mass (TOF) spectrometer (components from Jordan TOF Products, Inc.) is used for the detection of charged species formed using a tuneable ns UV-visible OPO laser (EKSPLA model-NT342B) accessing the 225 – 709 nm region, with 8 cm^{-1} pulse width and 10 Hz repetition rate. Although the wavelength step size is larger than that available with other systems (e.g. colorant lasers), the aim of this work is not to perform high precision spectroscopy as in previous studies, but rather to measure the spectral differences upon water complexation.

By optimising the timing of the pulses of both the supersonic valve and the laser, the gas phase species in the coldest part of the supersonic jet are photoexcited. This allows electronic spectra of vibrationally-cold neutral molecules and their clusters with water to be studied *via* two photon-one colour (1 + 1) photoionisation spectroscopy.

Calibration experiments involved a known standard, toluene, being run through the setup to calibrate the TOF measurements to m/z ratios and optimise the pulses. Toluene and all xylene species were purchased from Sigma-Aldrich at analytical standard purity. Water was deionised in-house.

Density-functional-theory (DFT) calculations were carried out using Gaussian16.[26] Equilibrium geometries and vibrational frequencies of the neutral monomer species and the clusters with water in the ground (S_0) and first excited state (S_1) were calculated at the CAM-B3LYP/aug-cc-pVDZ level of theory, including D3 Grimme's dispersion correction; these optimised geometries are shown in ESI Figure 1.[27] This level of theory has previously been used to successfully describe aromatic-water clusters, but the ωB97XD functional was also tested as a comparison using the same basis set. The ωB97XD calculations yielded no significant advantages over the coulomb attenuated method in either the optimised geometries or frequencies in the S_0 and S_1 states. The Franck-Condon factor simulations were also run for the monomers at this level of theory and very similar vibronic spectra were obtained to those run with the CAM-B3LYP functional. A larger basis set (aug-cc-pVTZ) was also tested using CAM-B3LYP. Although the triple zeta calculations gave slightly more symmetric optimised geometries for the 1:1 clusters, the calculations failed to converge for the 1:2 clusters. For consistency, it was therefore decided to run all calculations at the CAM-B3LYP/aug-cc-pVDZ level of theory.

The conformational space of all species was explored by optimising different starting geometries. Considering the symmetry of the xylene isomers and the water molecule, and the reduced size of the conformational landscape of the complex, the initial structures were selected to sample the structures presenting the most important interactions that can be found in this system (e.g. O-H $\cdots\pi$ ring, O$\cdots$H from methyl groups or aromatic hydrogens). Time-dependent density-functional-theory (TD-DFT) was used for the vertical excitation energies. Ground and excited state optimised geometries with zero-point energy (ZPE) correction were compared to derive the adiabatic transition energies. Non-covalent interactions (NCI) were revealed by means of the NCIPLOT program, which is based on the topological analysis and graphical interpretation of the electronic density and its derivatives, as well as the reduced density gradient.[28,29]

The topological analysis of the electronic density was also supported by applying the QTAIM method[30,31] as implemented in the AIMAll software (version 13.02.26).[32] In addition, the Natural Bonding Orbital (NBO) method was used to confirm the presence of intermolecular donor-acceptor interactions (H-bond type) and analyse the orbitals involved

therein.[33–35] The NBO 7.0 program[36] was employed for this purpose.

Vibrationally-resolved electronic spectra from the Frank-Condon transitions were simulated using the software package PGOPHER.[37] This software can be used to estimate the vibronic transitions by manually assigning quanta to individual vibrational modes in the excited state and then calculating the overlap integral between those filled S_1 modes and empty S_0 modes. Figure 1 is an example showing how the *meta*-xylene neutral monomer spectrum was assigned. For comparison with the vibrationally cold experimental spectra, these simulations were performed at 50 K, with a Lorentzian of width 10 cm^{-1}, and showed no significant changes at $\pm$ 50 K.

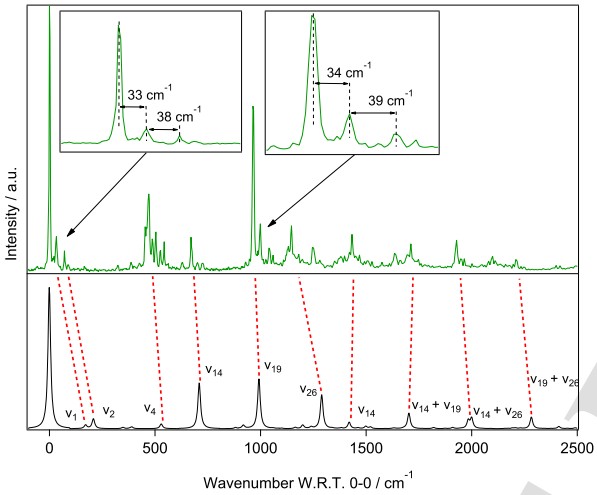

Figure 1 Experimental (green) and simulated (black) spectra for the *m*-xylene neutral monomer with the x-axis (energy) set to zero with respect to the 0-0 transition. Insets: torsional sub-structure of 0-0 (left) and ν_{19} (right) bands.

3 Results and Discussion

In order to understand the effects of the water molecules on the electronic structure of xylene, the neutral monomer species were first studied as benchmarking experiments. Aggregates of xylene with one and two water molecules were then generated to investigate how the binding of the water molecules changes the spectroscopy of the S_1 state, and in particular its vibrational sub-structure. In the case of *m*-xylene·$(H_2O)_n$, clusters up to n=5 were observed in the TOF measurement (ESI Figure 2). However, these larger aggregate species were not observed for all three xylene isomers, and those that were identified were of very low intensity. Thus, they were not further investigated and are not included in the following discussion. According to our theoretical simulations however, since the vertical ionisation potentials (VIP) for the different isomers do not substantially change as a result of complex formation i.e. exhibit a maximum variation of 0.28 eV (ESI Table 1), these clusters should be energetically accessible with the one-color REMPI (resonance-enhanced multiphoton ionisation) technique.

Experimental spectra for the S_1 electronic state of each of the xylene isomers in the monomer, 1:1 and 1:2 aggregates forms are presented in Figure 2. Below each of the spectra are the simulated vibronic spectra from PGOPHER. The assignments of these features are given in Tables 1, 2 and 3. Across all of the results, vastly different behaviour was observed for the three isomers, with some of the narrow bands in the monomer spectra becoming significantly broadened upon aggregation, while other species preserve their well defined structure regardless of the water binding.

3.1 Benchmarking the method with neutral monomers

The top three panels in Figure 2 show the neutral monomer experimental spectra for the three xylene isomers. The origin and the vibronic transitions display narrow bands with a spectral width of 10 cm^{-1} (consistent with the linewidth of the laser). The 0-0 transitions for *para*-, *meta*- and *ortho*-xylene appear at 36730 cm^{-1} (272.26 nm), 36949 cm^{-1} (270.64 nm) and 37308 cm^{-1} (268.04 nm) respectively - all of which are in good agreement with the literature values of Blease et al.[13,14] Experimental spectra over a greater energy range - between 36600 and 41000 cm^{-1} (273 and 244 nm) - are also shown in ESI Figure 3 with assignments given in ESI Table 2. A comparison of the origin transitions of the three isomers shows shifts of +219 and +359 cm^{-1} as the methyl position changes from *para* to *meta* to *ortho*. These shifts are a result of inductive effects from the methyl groups on the π electron system. In the case of *o*-xylene, the two methyl groups sit in such proximity to each other that there is a combination of attractive and repulsive interactions ESI Figure 4) which may also have an effect on the overall vibronic structure of the species.

For each of the neutral xylene monomers, a series of well-defined vibronic bands in Figure 2 indicates a minimal geometry change between the ground and excited states.[38] When comparing the PGOPHER simulated and experimental spectra, the band pattern is well reproduced and the blue shift observed in some of the simulated features (compared to the experimental spectra) is most likely due to the use of the harmonic potential approximation in our calculations, a phenomenon often corrected using a scaling factor. Looking more closely at the low energy features of the *m*-xylene neutral monomer (Figure 1), a distinct set of progression bands can be seen for the 0-0, ν_4 and ν_{19} bands. These sub-structure bands have similar separations of approximately +34 and +39 cm^{-1}. Hence it is suggested that these are low frequency modes coupling to the more intense vibrations, as previously reported by Blease et. al.[13,14] It can be seen by comparing the vibrational modes of the monomer species, that it is the same in-plane ring breathing and methyl torsion modes that are active for all three isomers. This suggests that the three isomers share a similar vibronic structure, which is tuned by inductive effects of the methyl groups.

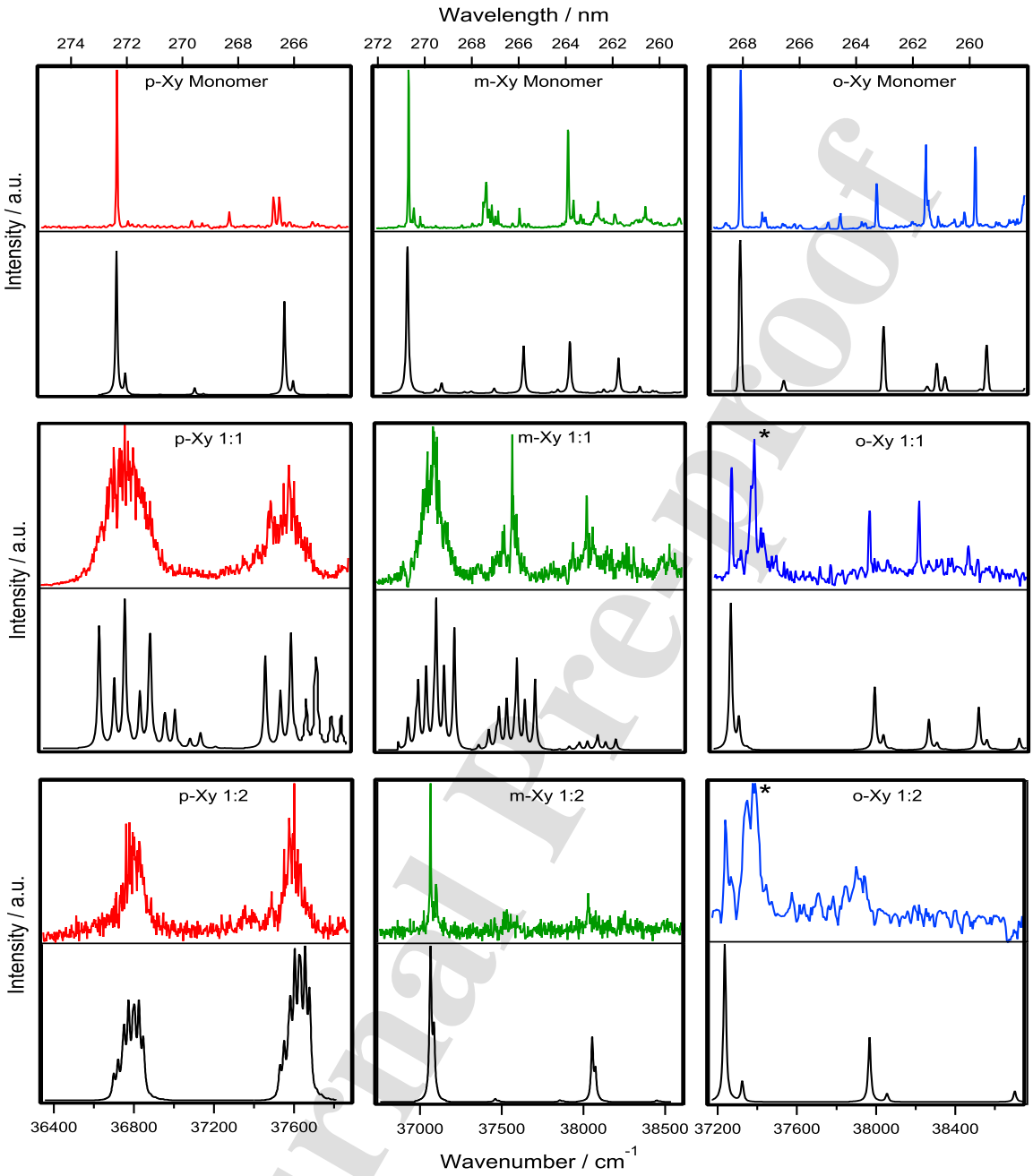

Figure 2 Experimental (coloured) and simulated (black) spectra for the neutral monomers and aggregate species. From left to right: *p*-xylene (red), *m*-xylene (green) and *o*-xylene (blue). From top to bottom: neutral monomers, 1:1 clusters, 1:2 clusters. It should be noted that the intensity scale is not the same in each panel. The asterisks in the *o*-xylene cluster spectra denote features attributed to evaporation effects as discussed in Section 3.4.

The vibronic spectra of the xylene monomers can also be compared to those of toluene and benzene, which contain one and zero methyl groups respectively. The 0-0 transition of toluene sits at 37476 cm^{-1} (ESI Figure 3), only 168 cm^{-1} higher than that for *o*-xylene.[39] Toluene and *o*-xylene both have electron density sitting on the methyl group(s) that are on one side of the aromatic ring system, and therefore have the highest dipole moments of all of the test species. In contrast to this, benzene has a 0-0 transition of 38086 cm^{-1},[40] which is 1356 cm^{-1} higher than that of *p*-xylene, despite both being apolar. This is to be expected however, as the lack of methyl groups on benzene means that there are no inductive effects on the π electron cloud which would lower the energy of the 0-0 transition.

Table 1 Position and assignments of the experimental and simulated vibronic bands for the *p*-xylene monomer, *p*-xylene·H_2O and *p*-xylene·$(H_2O)_2$. The width of broadened bands is given in parentheses. All values are in cm^{-1}. The assignment proposed by Blease et al. for the monomer is also included in parenthesis in the corresponding column. [14]

Experiment	Simulation	Mode	Assignment	Literature [14,16]
p-xylene monomer				
36730	0	0-0	Origin band (0_0^0)	36727
+54	43	ν_1 or ν_2 *	Methyl torsion	+55
+371	381	ν_4	Methyl bending ($9b_0^1$)	+370
+553	429	ν_8	In-plane ring breathing ($6a_0^1$)	+425
+799	830	ν_{17}	In-plane ring breathing ($16a_0^2$)	+802
p-xylene 1:1				
36767 (466)	0 (440)	0-0 + ν_2 + ν_6 + ν_8	Broadened origin band	-
+810 (409)	+828 (443)	ν_2 + ν_6 + ν_8 + ν_{23}	Broadened in-plane ring breathing	-
p-xylene 1:2				
36800 (263)	0 (238)	0-0 + ν_1 + ν_2	Broadened origin band	-
+ 802 (221)	824 (255)	ν_1 + ν_2 + ν_{29}	Broadened in-plane ring breathing	-

* ν_1 and ν_2 are very close in energy and both individually reproduce the experimental band when simulated in PGOPHER.

3.2 Spectral broadening of *p*-xylene-water clusters

The experimental and simulated spectra for the *p*-xylene-water clusters are shown in the first column of Figure 2 and ESI Figure 5, with assignments in Table 1. The spectra of both *p*-xylene·H_2O and *p*-xylene·$(H_2O)_2$ show significant broadening of the two features between 36400 and 37800 cm^{-1}.

Band widening in this type of experiment can have various explanations which can act independently, or in combination, to give rise to broad features, like those observed here. A common source of broadening is that the experimental observations are of vertical transitions rather than adiabatic transitions. Simultaneous excitation of a number of vibronic transitions then gives rise to a single, broad, structureless feature for a given electronic excited state. Another possible cause of band broadening is the effect of different conformations of a cluster being excited simultaneously. This would result in multiple vibronic transitions that are close in energy and appear as broad features. Lifetime broadening can also occur due to ultra-fast excited state processes. Finally, water molecules from the aggregates may also evaporate during the experiment, leading to spectral bands for higher order clusters being observed at masses corresponding to lower order clusters. This phenomenon has previously been reported in other systems, including pyrimidine–water clusters. [41] As a result of there being multiple possible broadening mechanisms, it is often difficult to determine exactly why the broad spectral features are observed.

In the case of *p*-xylene·H_2O and *p*-xylene·$(H_2O)_2$ (Figure 2, Table 1 and ESI Figure 5), the PGOPHER simulations provide compelling evidence for the broad features occurring as a result of low frequency modes coupling strongly to the most intense vibrations that were observed in the monomer case. For the *p*-xylene·H_2O cluster, the ν_2, ν_6 and ν_8 modes couple to the 0-0 and ν_{23} mode to give the observed features. This is also seen for the *p*-xylene·$(H_2O)_2$ species, but with the ν_1 and ν_2 modes in combination with the 0-0 and ν_{29} mode.

It is unlikely that the observed broadening is a result of multiple cluster conformations. The torsional modes of the CH_3 groups may have a subtle effect on the vibronic structure, but as no broadening of the features in the monomer spectra is observed, there is no reason to believe this would affect the bands of the clusters. Additionally, if different cluster conformers relating to the positioning of the H_2O molecules contributed to the broadening effect, then it would be expected that no single conformer would reproduce the observed spectrum. As each of the broad features in Figure 2 can be simulated with single cluster conformers, this does not seem to be the case. Furthermore, a similarly broad feature in the hole-burning spectroscopy study of phenol·$(H_2O)_2$ by Lipert and Colson was determined to be the effect of low frequency vibrations and explicitly ruled out as a result of multiple water complex conformers. [42] Evaporation of the *p*-xylene·$(H_2O)_2$ into the *p*-xylene·H_2O spectrum may also be present, but due to the overlap of the broad features, it is difficult to be certain. In both of the *p*-xylene-water cluster cases, the broad fea-

tures are therefore attributed to the low frequency modes being excited during the $S_1 \leftarrow S_0$ transition. These modes are shown in Figure 3.

3.3 Structural differences in *m*-xylene-water clusters

The experimental and simulated spectra for the *m*-xylene-water clusters are presented in the second column of Figure 2 and ESI Figure 6, with assignments in Table 2. For the *m*-xylene·H_2O species, three features between 36700 and 38600 cm^{-1} are observed, all three of which are subject to similar broadening effects as previously described for the *p*-xylene clusters. The PGOPHER simulation confirms that the low frequency modes responsible for this broadening are ν_2 and ν_4. These modes facilitate both the rotation of the methyl groups and the re-positioning of the water molecule above the aromatic ring. However, while the *m*-xylene·$(H_2O)_2$ cluster shows three broad features just above the baseline, the spectrum is dominated by an intense, narrow band at 37064 cm^{-1} as well as a less intense narrow feature at 38028 cm^{-1}. This suggests that while the $S_1 \leftarrow S_0$ transition of the 1:1 cluster involves the low frequency modes, the 1:2 cluster has a minimal geometry change between the ground and excited state. There is also some evidence for evaporation of the 1:2 cluster into the 1:1 species, as the peaks at 37064 and 38028 cm^{-1} in the *m*-xylene·$(H_2O)_2$ spectrum also appear in the *m*-xylene·H_2O spectrum.

3.4 Do *o*-xylene-water clusters have multiple geometries?

The *o*-xylene clusters behave somewhat differently to the *p*- and *m*- species, with no significant broadening observed for either the 1:1 or 1:2 aggregates (column three of Figure 2 and ESI Figure 7, with assignments in Table 3). PGOPHER simulations reproduce the intense features in the experimental spectra for both clusters without the inclusion of any low frequency modes. This suggests that in both cases, there is a minimal geometry change between the ground and excited state. However, both the *o*-xylene·$(H_2O)_2$ and *o*-xylene·H_2O experimental spectra show a slightly broad, intense band at 37374 cm^{-1} (marked with an asterisk in Figure 2) which does not appear in the monomer spectrum and cannot be reproduced by the PGOPHER simulation. When exploring the *o*-xylene·H_2O structure in the S_1 state, two minima were calculated with a ZPE corrected difference of 0.02 eV (~2 kJ/mol), within the accuracy limit of the method. These two structures (shown in Figure 4 as S_{1a} and S_{1b}) differ in that the H_2O molecule rotates by 90°. One hypothesis could thus be that the broad band represents a transition involving this S_{1b} geometry. PGOPHER simulations of the $S_{1b} \leftarrow S_0$ transition gave broad peaks at frequencies consistent with the observed peak, but that were 26 orders of magnitude lower in intensity than those simulated for the $S_{1a} \leftarrow S_0$ transition, ruling out the possibility of observing the $S_{1b} \leftarrow S_0$ transition. The intensities and positions of the observed *o*-xylene·H_2O vibronic progression thus indicates that we are experimentally observing the $S_{1a} \leftarrow S_0$ transition only. The peak at 37374 cm^{-1} could also belong to a transition between the S_{1b} structure and a second ground state minimum that was not found in our theoretical study. Re-optimisation of the S_{1b} geometry in the ground state reveals that this geometry is a transition state at the level of theory used in this study. The peak at 37374 cm^{-1} in both of the *o*-xylene clusters is therefore most likely attributed to evaporation from higher order *o*-xylene·$(H_2O)_n$ clusters.

3.5 Energetics and geometries for simulated clusters

The differences, both subtle and significant, between each of the xylene isomers' electronic spectra highlights the importance of the position of functional groups in the stabilisation of aromatic-water clusters. Further investigation of the ground and excited state structures derived computationally can be used to probe the energy of the $S_1 \leftarrow S_0$ transitions. The theoretical $S_1 \leftarrow S_0$ excitation energies are shown in Table 4. The results indicate that for all three isomers, the addition of one water molecule has only a small impact on these transition energies, the largest shift being 0.08 eV in the *o*-xylene isomer. It should be noted that the experimental trends observed for the 0-0 excitation energies are not precisely reproduced at the theoretical level used in this work (see Table 4). This is particularly true when comparing excitation energy values for different clusters of the same isomer. However, the maximum energy difference in these trends ($\sim$ 0.02 eV) are within the error range expected for these methods.

The equilibrium geometries of the complexes suggest that the shifts in excitation energy are most likely induced by O-H$\cdots\pi$ interactions between the water molecule and the π aromatic cloud in the ring. The topological analysis of the electronic density allows us to visualise these interactions. Both NCI and QTAIM methods show the presence of stabilising interactions between the O-H moiety from the water molecule and the π cloud in the aromatic ring. The NCI plots are shown in Figure 5, while the QTAIM analysis with bond critical points and bond paths is shown in ESI Figure 8. In the case of *m*-xylene·H_2O and *o*-xylene·H_2O complexes, there is an additional interaction between the oxygen atom of the water and the hydrogens from the methyl groups of xylene. This small interaction is more important for *o*-xylene because of the proximity of the methyl groups in the ring, which optimises a three-centre interaction. Note that NCI calculations such as these only offer a qualitative picture of the interactions that are present, and are not indicative of their strength or nature. However, this information is recovered from the NBO calculations which are discussed later.

Complexes with two water molecules were optimised starting from the addition of a water molecule to the 1:1 complex geometries previously obtained. Additional starting geometries were also explored. In all cases, the lowest energy structures were found to be those presenting a

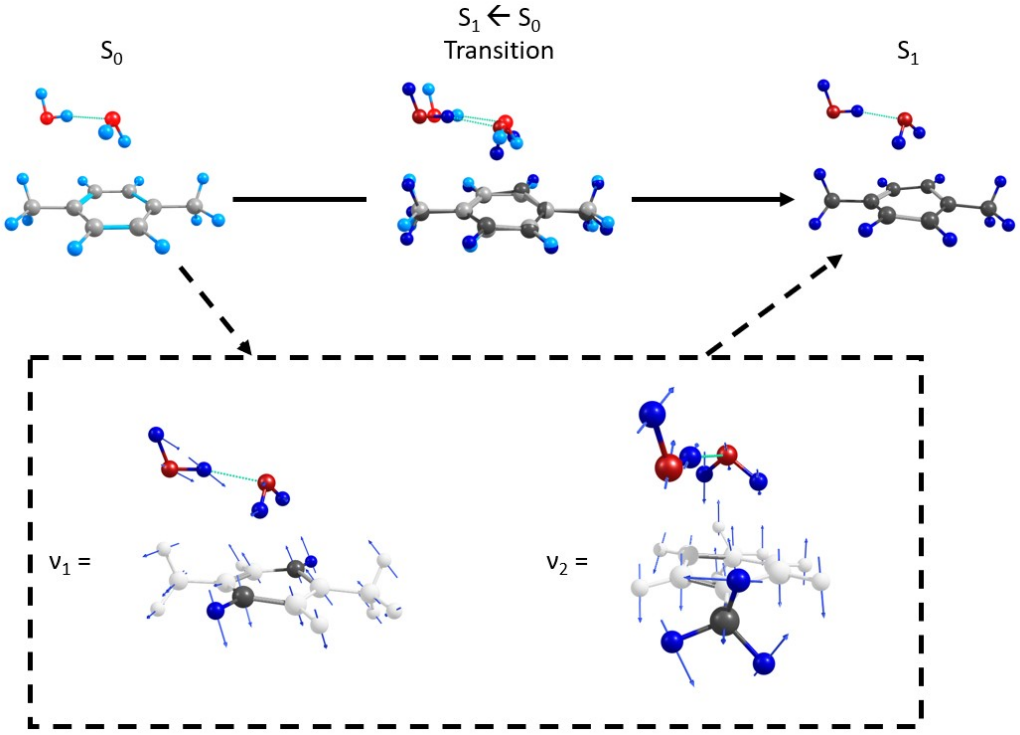

Figure 3 The change in geometry between the *p*-xylene·$(H_2O)_2$ S_0 and S_1 states and the ν_1 and ν_2 vibrations that allow the vibronic transition between these states. The structures and vibrations were calculated at the CAM-B3LYP/aug-cc-pVDZ level of theory.

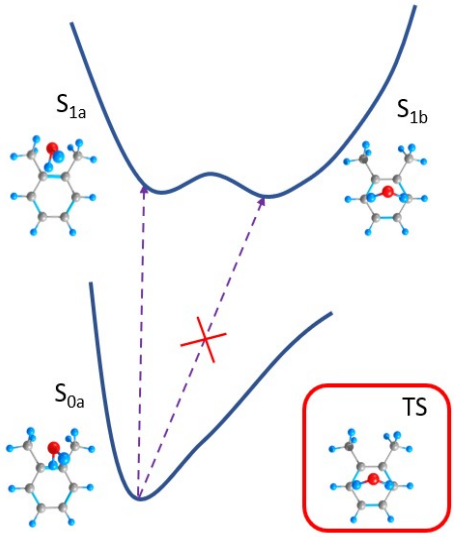

Figure 4 Schematic potential energy diagram for the different *o*-xylene·H_2O structures. S_{0a}, S_{1a} and S_{1b} were calculated as minima in the theoretical study, while the transition state was found rather than the expected S_{0b}.

strong hydrogen bond formed in the water dimer and an O-H$\cdots\pi$ interaction. In the case of the *o*-xylene 1:2 complex, the geometries in the ground and S_1 excited state are very similar. These two states are stabilised through the second water molecule forcing an optimal configuration for all of the possible interactions in the cluster, as observed through NCI, QTAIM and NBO methods (Figure 5, ESI Figures 8 and 9). This second water molecule increases the strength of the O-H$\cdots\pi$ interaction present in the 1:1 cluster, while adding an extra inter-water hydrogen bond. Furthermore, the 1:1 complex of this isomer is already the most stable, most likely due to the additional attractive interaction between water and the hydrogens from both methylic groups which is not observed for the other isomers.

NBO calculations reveal how the donor/acceptor NBO orbitals differ between the complexes and the strength of their interaction (ESI Figure 9). Note that energy values obtained by the NBO method are not the true values of the interaction energy within the cluster, but serve as an indication of their strength. The results confirm the presence of weak interactions ($\sim$ 8 kJ/mol) in all of the complexes, mainly between the π bonding C-C orbitals from the aromatic ring and the σ^* antibonding O-H orbitals from the water moiety. The strength of this interaction increases slightly when 1:2 complexes are formed. In addition, contributions from σ_{OH} - π^*_{C-C} interactions are also involved in the *o*-xylene·H_2O 1:1 complex. NBO calculations also reveal the strong ($\sim$ 67 kJ/mol) hydrogen-bond interaction (n_{O_1} - $\sigma^*_{O_2-H}$) between the water molecules in the 1:2 complexes. Finally, the n_O - σ^*_{C-H} interaction ($\sim$ 4 - 17 kJ/mol) between the lone pair of the water oxygen and the C-H orbitals of the methyl groups is also observed, being more important in the case of *o*-

Table 2 Position and assignments of the experimental and simulated vibronic bands for the *m*-xylene monomer, *m*-xylene·H_2O and *m*-xylene·$(H_2O)_2$. The width of broadened bands is given in parentheses. All values are in cm^{-1}. The assignment proposed by Blease et al. for the monomer is also included in parenthesis in the corresponding column. [14]

Experiment	Simulation	Mode	Assignment	Literature [14,16]
m-xylene monomer				
36949	0	0-0	Origin band (0_0^0)	36950
+33	170	ν_1	Methyl torsion	+32
+71	208	ν_2	Methyl torsion	+73
+470	528	ν_4	Methyl torsion	-
+670, +1432	714, 1418	ν_{14}	In-plane ring breathing (1_0^1)	-
+964	994	ν_{19}	In-plane ring breathing (12_0^1)	-
+1146	1288	ν_{26}	In-plane ring breathing (13_0^1)	-
m-xylene 1:1				
37097 (284)	0 (347)	0-0 + ν_2 + ν_4	Broadened origin band	-
+480 (144), +928 (114)	463 (295), 928 (253)	ν_2 + ν_4 + ν_{15}	Broadened ring deformation	-
m-xylene 1:2				
37064	0	0-0	Origin band	-
+33	20	ν_1	Water rocking	-
+467	392	ν_{17}	Ring deformation	-
+964	989	ν_{31}	In-plane ring breathing	-

xylene, where the interaction between the water molecule oxygen atom and both of the methyl groups is maximised.

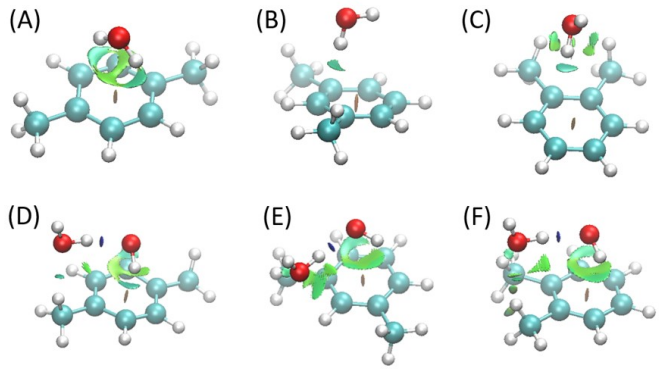

Figure 5 NCIPLOT calculated surfaces in the ground state for; (A) *p*-xylene·H_2O, (B) *m*-xylene·H_2O, (C) *o*-xylene·H_2O, (D) *p*-xylene·$(H_2O)_2$, (E) *m*-xylene·$(H_2O)_2$, (F) *o*-xylene·$(H_2O)_2$. Steric repulsion is shown in orange at the centre of the aromatic rings, dispersion interactions are shown in green and hydrogen bonds between water molecules are shown in blue.

3.6 Comparison with other aromatic-water clusters

Several other studies have investigated the electronic effects of water on aromatics in clusters. Theoretical studies by Simon et al. found that the geometry of interaction of an aromatic molecule with water can have a considerable impact on the VIP of the aromatic. [43,44] An initial DFTB study by the authors determined that the VIP of an aromatic adsorbed on a water cluster could increase or decrease, depending on whether the PAH interacts with the water via the π cloud of the aromatic ring system or via the hydrogens at the edge of the molecule, respectively. [43] A more recent, higher level TD-DFT and MS-CASPT2 study concluded that a side-on attachment of a water molecule (from a hexagonal ice structure) to a benzene monomer had the effect of lowering the VIP by as much as -0.33 eV, while a water molecule bound through the π cloud of the aromatic ring increased the VIP by +0.32 eV. [44] These shifts are consistent with those calculated in this work, supporting the conclusion that the water binds through the π cloud of the xylene monomer.

Toluene·$(H_2O)_n$ clusters were investigated by Li et al. through one-color mass resolved excitation spectroscopy. [45] In this study, it was found that the origin band was blue shifted by 15 cm^{-1} as the toluene·$(H_2O)_n$ cluster size increased from n=1 to 3 due to the inductive effects of the

Table 3 Position and assignments of the experimental and simulated vibronic bands for the *o*-xylene monomer, *o*-xylene·H_2O and *o*-xylene·H_2O. All values are in cm^{-1}. The assignment proposed by Blease et al. for the monomer is also included in parenthesis in the corresponding column.[14]

Experiment	Simulation	Mode	Assignment	Literature[14,16]
o-xylene monomer				
37308	0	0-0	Origin band (0_0^0)	37308
+109	126	ν_3	Methyl torsion	
+689	729	ν_{15}	In-plane ring breathing (1_0^1)	+693
+942	1001	ν_{20}	In-plane ring breathing ($18b_0^1$)	+940
+1192	1253	ν_{26}	In-plane ring breathing ($7a_0^1$)	+1196
o-xylene 1:1				
37262	0	0-0	Origin band	-
+114	-	-	Unknown	-
+696	726	ν_{21}	In-plane ring breathing	-
+947	999	ν_{26}	In-plane ring breathing	-
+1195	1250	ν_{32}	In-plane ring breathing	-
o-xylene 1:2				
37238	0	0-0	Origin band	-
+134	-	-	Unknown	-
+660	731, 1467	ν_{25}	In-plane ring breathing	-

Table 4 Excitation energies for the first excited state of the xylene monomers, 1:1 and 1:2 clusters. All calculated using TD-DFT at the CAM-B3LYP/aug-cc-pVDZ level of theory in the adiabatic case. Vertical energies are presented in parentheses.

	Excitation Energy / eV		
	Monomer	1:1	1:2
para	4.942 (5.243)	4.913 (5.218)	4.876 (5.291)
meta	4.991 (5.285)	4.975 (5.288)	4.991 (5.300)
ortho	5.059 (5.343)	5.056 (5.410)	4.977 (5.294)

water molecules. This is a similar shift in energy to that observed for the *o*-xylene clusters in this work, with the 0-0 transition blue shifting by 24 cm^{-1} between n=1→2. Although similar shifts may be present for the *p*- and *m*-xylene clusters, the broadening of the bands in the 1:1 (*para*- and *meta*) and 1:2 (*para*-) cluster spectra make it difficult to be certain if the origin peak has shifted in energy or broadened to appear at a different wavenumber.

Spectroscopic studies of water clusters with phenol and *p*-cresol have previously shown that broad vibronic bands in the aromatic·$(H_2O)_2$ spectra are a result of the cluster geometry changing during the $S_1 \leftarrow S_0$ transition from a cyclic hydrogen bonded ground state to a linear hydrogen bonded excited state.[46,47] In the case of phenol and cresol, the water molecules bind directly to the OH group on the aromatic ring, as opposed to the π system of the xylenes, but the role of the low frequency, inter-molecular vibrational modes is still the most likely cause of the broadening observed in the xylene cluster spectra of this work.

4 Conclusions and Perspectives

These experiments and accompanying theoretical calculations have provided fundamental molecular physics data on the S_1 electronic energy levels and their vibrational substructure for xylene-water clusters, providing insights into the growth and reactivity of these clusters. The experimental spectra for the *p*-xylene·H_2O, *p*-xylene·$(H_2O)_2$ and *m*-xylene·H_2O aggregates show broadening of the vibronic features. These broad bands have been simulated using PGOPHER to assign the combination bands and begin to attribute the broadening phenomena to a combination of three physical effects:

- Low frequency modes involving the water molecule rocking motions coupling to the intense vibronic progressions of the origin band and the aromatic ring deformation.

- More than one minimal energy geometry in either the S_0 or S_1 or both, giving rise to multiple sets of vibronic progressions.
- Evaporation of a water molecule from the clusters, therefore observing spectral features from larger clusters in the spectra of the 1:2 and 1:1 aggregates.

Theoretical studies provide an explanation for this behaviour, with the electron density remaining on the methyl groups during the excitation of the *o*-xylene-water clusters instead of shifting to the aromatic ring system to interact with the water molecule – as is the case for the *m*- and *p*-xylene-water clusters. By describing the changes in electronic behaviour between the three xylene isomers, this study of xylene-water complexes shows that the position of the methyl functional groups significantly impacts the solvation of aromatics in water.

These findings are important in the context of atmospheric chemistry, as the lifetime of pollutants in the mesosphere is dependant on the water solvation of these species in the gas phase. By understanding the fundamental physics which dictates the binding of this solvation, theoretical models can better describe how atmospheric chemistry evolves over time as a function of pollutant density.

The work described here is also a first step towards a wider study of the thermodynamic/electronic properties and spectroscopy of xylene isomers adsorbed on and in water ices. These ice systems are important in astrochemical studies as it is thought that PAHs and smaller hydrocarbons such as benzene, toluene and xylene could be present in water-dominated icy mantles on dust grains in dense molecular clouds.[48] In astrochemical environments, UV irradiation is thought to play an important role in the chemical evolution of molecular ices adsorbed onto dust grain surfaces. In these low temperature and pressure environments, the rules of reactive chemistry completely change and subtle changes in the electronic structure of gas phase species and surface adsorbed molecules can be the difference between the formation of new species and the desorption of unreacted ices. As shown, the aggregation of water molecules to the xylene monomers has the effect of lowering the excitation energy by as much as 0.08 eV. This reduction in energy may seem negligible in most contexts, but when considering the extremely low energy environments of the interstellar medium, this shift could allow for previously inaccessible reaction pathways to open. The results reported here will form the basis for a study of the UV-Visible spectroscopy of solid xylene-water ices using a newly developed, ultra-high vacuum compatible, optical spectrometer.[49,50]

Author Contributions

The project was initiated and managed by WAB and JAN. Experiments were performed by JEF, AGQ, GAP, AH, AN and JAN. Theoretical calculations were performed by JEF, AGQ and JAN. The manuscript was written by JEF and AGQ, with assistance from WAB, GAP and JAN. All authors contributed to data interpretation and commented on the paper.

Acknowledgements

The Science and Technology Facilities Council (STFC) are acknowledged for a studentship for JEF. This article is based upon work carried out during a Short-Term Scientific Mission (STSM) funded by COST Action CA18212 – Molecular Dynamics in the GAS phase (MD-GAS), supported by COST (European Cooperation in Science and Technology). We acknowledge the use of the high-performance computing facility, Apollo2, at the University of Sussex and the computing centre MésoLUM managed by ISMO (UMR8214) and LPGP (UMR8578), University Paris-Saclay (France). JAN acknowledges funding from the Agence Nationale de la Recherche (ANR, HYDRAE project ANR-21-CE30-0004-01). JAN and AN acknowledge the Origins Institute; the project leading to this publication has received funding from Excellence Initiative of Aix-Marseille University - A*MIDEX, a French "Investissements d'Avenir" programme (AMX-21-IET-018, Origines). The authors thank Christophe Jouvet, John Turner and Karinne Miqueu for helpful discussions.

References

[1] A. Zalel, Yuval and D. M. Broday, *Environmental Pollution*, 2008, **156**, 553–562.

[2] T. M. Sack, D. H. Steele, K. Hammerstrom and J. Remmers, *Atmospheric Environment. Part A. General Topics*, 1992, **26**, 1063–1070.

[3] H. M. Daly and A. B. Horn, *Physical Chemistry Chemical Physics*, 2009, **11**, 1069–1076.

[4] G. D. G. Peña, M. M. Alrefaai, S. Y. Yang, A. Raj, J. L. Brito, S. Stephen, T. Anjana, V. Pillai, A. A. Shoaibi and S. H. Chung, *Combustion and Flame*, 2016, **172**, 1–12.

[5] X. M. Zhou, J. W. Liu, M. E. Zhang and S. J. Chen, *Talanta*, 1998, **46**, 757–760.

[6] E. Herbst and E. F. van Dishoeck, *Annual Review of Astronomy and Astrophysics*, 2009, **47**, 427–480.

[7] D. A. Williams and E. Herbst, *Surface Science*, 2002, **500**, 823–837.

[8] C. Walsh, T. J. Millar, H. Nomura, E. Herbst, S. W. Weaver, Y. Aikawa, J. C. Laas and A. I. Vasyunin, *Astronomy and Astrophysics*, 2014, **563**, 33.

[9] D. V. Chakarov, L. Österlund and B. Kasemo, *Vacuum*, 1995, **46**, 1109–1112.

[10] S. V. Anantakrishnan and D. S. Rao, *Proceedings of the Indian Academy of Sciences - Section A 1964 60:3*, 1964, **60**, 201–210.

[11] H. Kanai, V. Inouye, L. Yazawa, R. Goo and H. Wakatsuki, *Journal of Chromatographic Science*, 2005, **43**, 57–62.

[12] H. M. Cuppen, E. Herbst and Q. Chang, *Journal of Physics Conference Series*, 2005, **6**, 18.

[13] T. G. Blease, *Laser Multiphoton Ionization Spectroscopy and Analysis of the Xylene Isomers*, 1985.

[14] T. G. Blease, R. J. Donovan, P. R. R. Langridge-Smith and T. Ridley, *Laser Chemistry*, 1988, **9**, 241–263.

[15] P. J. Breen, J. A. Warren, E. R. Bernstein and J. I. Seeman, *Journal of Chemical Physics*, 1987, **87**, 1917.

[16] T. Ebata, Y. Suzuki, N. Mikami, T. Miyashi and M. Ito, *Chemical Physics Letters*, 1984, **110**, 597–601.

[17] A. B. Stephansen and T. I. Sølling, *Structural Dynamics*, 2017, **4**, 044008.

[18] Y. Z. Liu, S. R. Xiao, K. Gregor and G. Thomas, *Chinese Physics Letters*, 2014, **31**, 127802.

[19] H. D. Barth, K. Buchhold, S. Djafari, B. Reimann, U. Lommatzsch and B. Brutschy, *Chemical Physics*, 1998, **239**, 49–64.

[20] B. Brutschy, C. Janes and J. Eggert, *ChemInform*, 1988, **19**, 71–81.

[21] A. L. Sobolewski, W. Domcke, C. Dedonder-Lardeux and C. Jouvet, *Physical Chemistry Chemical Physics*, 2002, **4**, 1093–1100.

[22] M. I. Taccone, A. F. Cruz-Ortiz, J. Dezalay, S. Soorkia, M. Broquier, G. Grégoire, C. G. Sánchez and G. A. Pino, *Journal of Physical Chemistry A*, 2019, **123**, 7744–7750.

[23] J. Noble, C. Dedonder-Lardeux and C. Jouvet, *Excited States Processes in Protonated Molecules Studied by Frequency-Domain Spectroscopy*, Springer Singapore, 2019, pp. 337–365.

[24] A. Simon, J. A. Noble, G. Rouaut, A. Moudens, C. Aupetit, C. Iftner and J. Mascetti, *Physical Chemistry Chemical Physics*, 2017, **19**, 8516–8529.

[25] J. A. Noble, C. Jouvet, C. Aupetit, A. Moudens and J. Mascetti, *Astronomy and Astrophysics*, 2017, **599**, 1–6.

[26] M. J. Frisch, G. W. Trucks, H. B. Schlegel, G. E. Scuseria, M. A. Robb, J. R. Cheeseman, G. Scalmani, V. Barone, G. A. Petersson, H. Nakatsuji, X. Li, M. Caricato, A. V. Marenich, J. Bloino, B. G. Janesko, R. Gomperts, B. Mennucci, H. P. Hratchian, J. V. Ortiz, A. F. Izmaylov, J. L. Sonnenberg, D. Williams-Young, F. Ding, F. Lipparini, F. Egidi, J. Goings, B. Peng, A. Petrone, T. Henderson, D. Ranasinghe, V. G. Zakrzewski, J. Gao, N. Rega, G. Zheng, W. Liang, M. Hada, M. Ehara, K. Toyota, R. Fukuda, J. Hasegawa, M. Ishida, T. Nakajima, Y. Honda, O. Kitao, H. Nakai, T. Vreven, K. Throssell, J. M. J. A., J. E. Peralta, F. Ogliaro, M. J. Bearpark, J. J. Heyd, E. N. Brothers, K. N. Kudin, V. N. Staroverov, T. A. Keith, R. Kobayashi, J. Normand, K. Raghavachari, A. P. Rendell, J. C. Burant, S. S. Iyengar, J. Tomasi, M. Cossi, J. M. Millam, M. Klene, C. Adamo, R. Cammi, J. W. Ochterski, R. L. Martin, K. Morokuma, O. Farkas, J. B. Foresman and D. J. Fox, *Gaussian 16*, 2016.

[27] S. Grimme, *Journal of Computational Chemistry*, 2004, **25**, 1463–1473.

[28] E. R. Johnson, S. Keinan, P. Mori-Sánchez, J. Contreras-García, A. J. Cohen and W. Yang, *Journal of the American Chemical Society*, 2010, **132**, 6498–6506.

[29] J. Contreras-García, E. R. Johnson, S. Keinan, R. Chaudret, J. Piquemal, D. N. Beratan and W. Yang, *J Chem Theory Comput.*, 2011, **7**, 625–632.

[30] R. F. W. Bader, *Chem. Rev.*, 1991, **91**, 893–928.

[31] R. F. W. Bader, *Atoms in molecules : a quantum theory*, Oxford : Clarendon press, 1990.

[32] K. , Todd A., *AIMAll*, 2019, `aim.tkgristmill.com`.

[33] A. E. Reed, L. A. Curtiss and F. Weinhold, *Chemical Reviews*, 1988, **88**, 899–926.

[34] A. E. Reed and F. Weinhold, *J. Chem. Phys.*, 1985, **83**, 1736–1740.

[35] J. P. Foster and F. Weinhold, *J. Am. Chem. Soc.*, 1980, **102**, 7211–7218.

[36] E. D. Glendening, J. K. Badenhoop, A. E. Reed, J. E. Carpenter, J. A. Bohmann, C. M. Morales, P. Karafiloglou, C. R. Landis and F. Weinhold, *NBO 7.0*, 2018.

[37] C. M. Western, *Journal of Quantitative Spectroscopy and Radiative Transfer*, 2017, **186**, 221–242.

[38] J. A. Noble, E. Marceca, C. Dedonder, W. Phasayavan, G. Féraud, B. Inceesungvorn and C. Jouvet, *Physical Chemistry Chemical Physics*, 2020, **22**, 27280–27289.

[39] C. J. Seliskar, M. Heaven and M. A. Leugers, *Journal of Molecular Spectroscopy*, 1983, **97**, I86– 193.

[40] K. O. Börnsen, S. H. Lin, H. L. Selzle and E. W. Schlag, *Journal of Chemical Physics*, 1989, **90**, 1299–1306.

[41] X. Huang, J.-P. Aranguren, J. Ehrmaier, J. A. Noble, W. Xie, A. L. Sobolewski, C. Dedonder-Lardeux, C. Jouvet and W. Domcke, *Physical Chemistry Chemical Physics*, 2020, **22**, 12502–12514.

[42] R. J. Lipert and S. D. Colson, *Chem. Phys. Lett.*, 1989, **161**, 303–307.

[43] E. Michoulier, N. Ben Amor, M. Rapacioli, J. A. Noble, J. Mascetti, C. Toubin and A. Simon, *Physical Chemistry Chemical Physics*, 2018, **20**, 11941–11953.

[44] N. Ben Amor, E. Michoulier and A. Simon, *Theoretical Chemistry Accounts*, 2021, **140**, 70.

[45] S. Li and E. R. Bernstein, *Journal of Chemical Physics*, 1992, **97**, 792.

[46] M. Pohl, M. Schmitt and K. Kleinermanns, *Journal of Chemical Physics*, 1991, **94**, 1717.

[47] K. Kleinermanns, M. Gerhards and M. Schmitt, *Ber. Bunsenges. Phys. Chem.*, 1997, **101**, 1785–1798.

[48] V. C. Geers, E. F. van Dishoeck, K. M. Pontoppidan, F. Lahuis, A. Crapsi, C. P. Dullemond and G. A. Blake, *Astronomy and Astrophysics*, 2009, **495**, 837–846.

[49] J. W. Stubbing, T. L. Salter, W. A. Brown, S. Taj and M. R. S. McCoustra, *Review of Scientific Instruments*, 2018, **89**, 054102.

[50] J. W. Stubbing, M. R. S. McCoustra and W. A. Brown, *Physical Chemistry Chemical Physics*, 2020, **22**, 25353–25365.

Gas phase electronic spectra of xylene-water aggregates Manuscript number: JMSP-D-22-00233

Highlights

- Experimental gas phase electronic spectra of xylene-water aggregates are reported for the first time.
- PGOPHER has been used to simulate the vibronic spectra of xylene-water aggregates from calculated geometries and frequencies.
- The vibronic spectra of *p*-xylene·H_2O, *p*-xylene·$(H_2O)_2$ and *m*-xylene·H_2O show significant broadening due to low frequency vibrational modes coupling to the intense vibronic progressions.
- Evaporation of water molecules from higher order clusters may also be responsible for peak broadening.
- NCI, NBO and QTAIM calculations describe the relative stability of the xylene-water clusters.

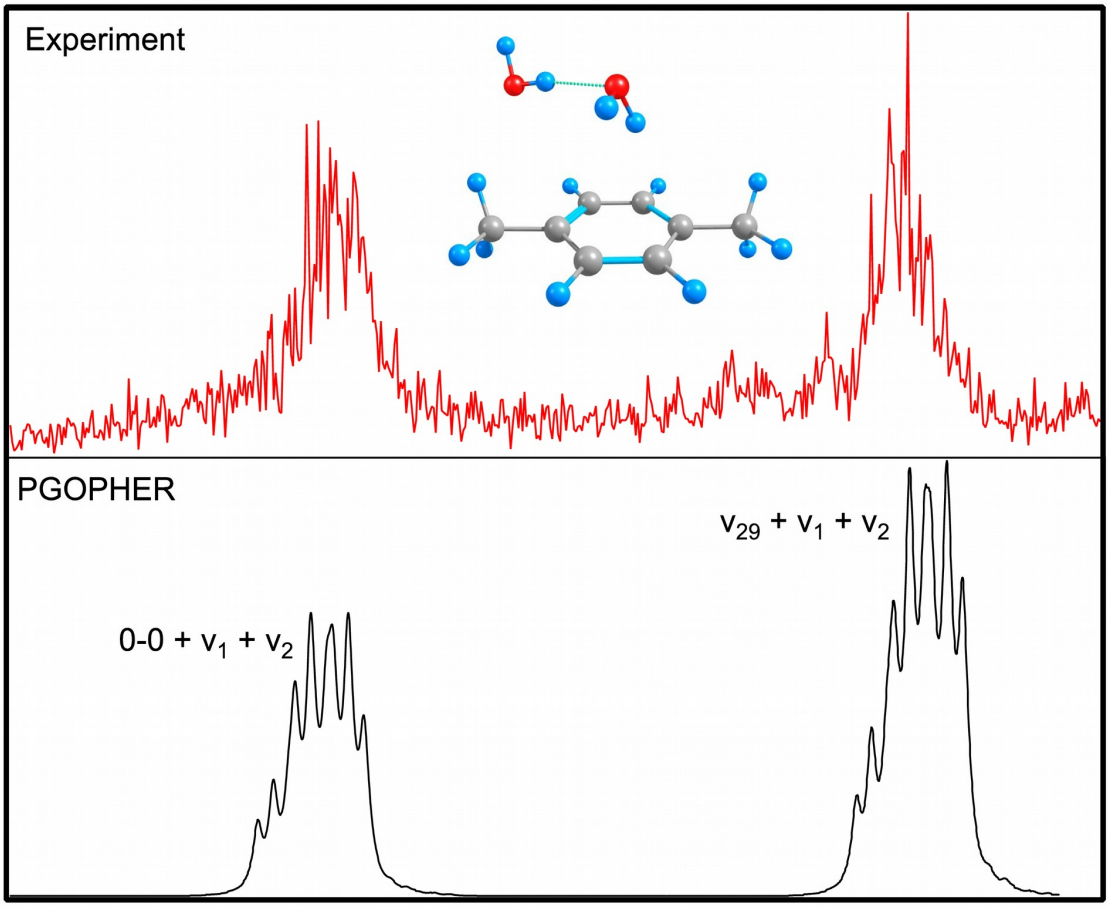
Experiment
PGOPHER
0-0 + ν_1 + ν_2
ν_{29} + ν_1 + ν_2

Author statement for JMSP-D-2022-00233

The project was initiated and managed by WAB and JAN. Experiments were performed by JEF, AGQ, GAP, AH, AN and JAN. Theoretical calculations were performed by JEF, AGQ and JAN. The manuscript was written by JEF and AGQ, with assistance from WAB, GAP and JAN. All authors contributed to data interpretation and commented on the paper.

Declaration of interests

☒ The authors declare that they have no known competing financial interests or personal relationships that could have appeared to influence the work reported in this paper.

☐ The authors declare the following financial interests/personal relationships which may be considered as potential competing interests: